AGU PUBLICATIONS

JGR

Journal of Geophysical Research: Oceans

RESEARCH ARTICLE

10.1002/2016JC012178

Storm surge along the Pacific coast of North America

Peter D. Bromirski[1], Reinhard E. Flick[2], and Arthur J. Miller[3]

[1]Scripps Institution of Oceanography, University of California, San Diego, La Jolla, California, USA, [2]California State Parks Division of Boating and Waterways, Scripps Institution of Oceanography, La Jolla, California, USA, [3]Scripps Institution of Oceanography, La Jolla, California, USA

Supporting Information:
• Supporting Information S1

Correspondence to:
P. D. Bromirski,
pbromirski@ucsd.edu

Citation:
Bromirski, P. D., R. E. Flick, and A. J. Miller (2016), Storm surge along the Pacific coast of North America, *J. Geophys. Res. Oceans*, *121*, doi:10.1002/2016JC012178.

Received 25 JUL 2016
Accepted 4 NOV 2016
Accepted article online 11 NOV 2016

Abstract Storm surge is an important factor that contributes to coastal flooding and erosion. Storm surge magnitude along eastern North Pacific coasts results primarily from low sea level pressure (SLP). Thus, coastal regions where high surge occurs identify the dominant locations where intense storms make landfall, controlled by storm track across the North Pacific. Here storm surge variability along the Pacific coast of North America is characterized by positive nontide residuals at a network of tide gauge stations from southern California to Alaska. The magnitudes of mean and extreme storm surge generally increase from south to north, with typically high amplitude surge north of Cape Mendocino and lower surge to the south. Correlation of mode 1 nontide principal component (PC1) during winter months (December–February) with anomalous SLP over the northeast Pacific indicates that the dominant storm landfall region is along the Cascadia/British Columbia coast. Although empirical orthogonal function spatial patterns show substantial interannual variability, similar correlation patterns of nontide PC1 over the 1948–1975 and 1983–2014 epochs with anomalous SLP suggest that, when considering decadal-scale time periods, storm surge and associated tracks have generally not changed appreciably since 1948. Nontide PC1 is well correlated with PC1 of both anomalous SLP and modeled wave height near the tide gauge stations, reflecting the interrelationship between storms, surge, and waves. Weaker surge south of Cape Mendocino during the 2015–2016 El Niño compared with 1982–1983 may result from changes in Hadley circulation. Importantly from a coastal impacts perspective, extreme storm surge events are often accompanied by high waves.

1. Introduction

The greatest societal impacts from coastal storm activity result when high waves coincide with high total water level, producing coastal flooding as well as beach and sea cliff erosion, and affecting coastal infrastructure. Total water level includes tide and storm surge, both superimposed on mean regional sea level (RSL), with the additional factors of wave setup/runup contributing to coastal impacts. Impacts of wave activity in coastal regimes will be exacerbated by anticipated global warming-related sea level rise, which allows more wave energy to reach farther shoreward. Although substantial interannual RSL variability has occurred along the eastern boundary of the North Pacific over the last four decades, which is largely related to El Niño/Southern Oscillation (ENSO) episodes and Pacific Decadal Oscillation (PDO) [*Mantua et al*., 1997] variations, the trend in RSL was relatively stationary along the Pacific coast of North America from about 1980 to 2011 [*Bromirski et al*., 2011]. However, a recent study by *Hamlington et al*. [2016] indicates that North Pacific eastern boundary sea levels are now rising, affirming the anticipated resumption of RSL rise by *Bromirski et al*. [2011]. Rising RSL will amplify coastal impacts during strong winter storms [*Cayan et al*., 2008; *Bromirski et al*., 2012], of which storm surge can be a significant contributor when total water levels (combined with waves) approach critical thresholds. Thus, understanding and anticipating storm surge characteristics and trends is important for coastal planning and establishing design criteria for future coastal development, as well as being an indicator of potential changes resulting from anthropogenically forced climate warming.

Extratropical cyclone activity over the North Pacific has been assessed by several studies that apply different cyclone tracking methods [e.g., *Graham and Diaz*, 2001; *Ulbrich et al*., 2009; *Wang et al*., 2013] to 6-hourly reanalysis sea level pressure (SLP) fields. These tend to show an increase in cyclone activity in the high midlatitudes of the North Pacific, with mixed trends along the Pacific coast of North America. Unlike these

studies, here we study sea level height fluctuations extracted from hourly tide gauge measurements to characterize coastal storm activity. Because North Pacific cyclones tend to turn northward as they mature and to decay as they move eastward [*Anderson and Gyakum*, 1989], the impact of increased cyclone activity in the central North Pacific on the U.S. West coast depends on a storm's behavior in the near-coastal eastern Pacific, which may differ substantially from its open ocean characteristics. Thus, direct measures of storminess along the eastern North Pacific coasts are invaluable for gauging coastal vulnerability to climate variability.

Storm surge results primarily from variations in SLP that produce an "inverse barometer" effect, causing water levels to rise under low SLP and be depressed under high SLP. SLP has been shown to be well correlated to surge levels, but poorly correlated to local wind speed [*Bromirski et al*., 2003], indicating that the inverse barometer effect provides the dominant contribution to storm surge along the U.S. Pacific coast. The water level response to meteorological events depends on the location of the center of the low relative to the tide gauge, the SLP gradient (and associated wind speed and direction), and the rate of storm movement. Consequently, the meteorologically forced water level fluctuations at coastal locations depend on where the storm center makes landfall, determined by the underlying dominant storm track across the North Pacific that directs storms to particular coastal locations. Thus, the spatial distribution of storm surge extremes along the northeastern Pacific coast is an important consideration in identifying changes in the spatial distribution of storm landfalls in this coastal region.

In contrast, surge levels can be much higher along the much wider, shallow continental shelves along the U.S. East and Gulf Coasts than the U.S. West coast due to wind-driven wind setup. This occurs particularly when tropical cyclones (hurricanes) make landfall. The typically much higher hurricane wind speeds combined with the shelf morphology produce greater wind setup that dominates surge levels, in contrast to generally lower wind speed eastern North Pacific storms where SLP dominates surge. Along the U.S. Pacific coast, storm track and storm intensity are key factors, producing nontidal residuals north of Cape Mendocino that are generally comparable to surge levels along the U.S. East and Gulf coasts [*Menéndez and Woodworth*, 2010].

2. Data and Methods

Robust measures of the long-term spatial and temporal variability of storm surge along the Pacific coast of North America can be estimated from hourly tide gauge observations, which provide consistent hourly sea level measurements spanning multidecadal periods. The broad station distribution and long-duration records reduce uncertainties in long-term comparisons of the sea level response to near-coastal storm behavior. Storm surge in this study was estimated from nontide variability determined following *Bromirski et al*. [2003]. This methodology spectrally removes the tides and other water level variations (including most of the mean RSL and PDO-related sea surface (SST) temperature effects after demeaning and detrending) at periods greater than about 6 months, leaving nontide sea level fluctuations dominated nearly entirely by synoptic-scale variability.

Because positive nontidal (storm surge) sea level fluctuations are forced largely by low SLP and wind variations [*Chelton and Davis*, 1982] and are associated with precipitation [*Bromirski et al*., 2003], meteorologically forced water level variation gives a useful composite estimate of storminess. Unlike reanalysis datasets that have bias issues prior to the satellite era [*Chang*, 2007; *Sterl*, 2004], tide gauge nontide sea level estimates provide an unbiased stable-platform climate-related time series of sufficient duration to investigate long-term spatial patterns of storminess climate variability along the Pacific coast of North America. Also, the hourly sampling rate allows better characterization of synoptic events than more coarsely sampled reanalysis SLP and precipitation data, the latter generally available only at daily resolution.

Hourly tide gauge data were obtained from the National Oceanic and Atmospheric Administration (NOAA) National Ocean Service (NOS) Center for Operational Oceanographic Products and Services (Co-Ops) and the University of Hawaii Sea Level Center. Other data used in this study include 6-hourly NOAA National Centers for Environmental Prediction (NCEP) reanalysis SLP, obtained from the NOAA National Climate Data Center (NCDC). Also employed are hindcast WAVEWATCH III version 3.14 (WW3) [*Tolman*, 2009] wave model significant wave height (*Hs*) data forced by NOAA National Centers for Environmental Prediction (NCEP) reanalysis project [*Kalnay et al*., 1996] global near-surface winds. Model wave data were saved at 6 h

intervals with a spatial resolution of 1.0° × 1.0° latitude/longitude and spanning 1948–2008, as described in *Bromirski et al*. [2013]. The hourly tide gauge data allow for a more detailed description of coastal storminess variability than 6-hourly reanalysis SLP and wave model *Hs*.

Empirical orthogonal function (EOF) analyses were employed to identify the dominant modes of nontide (storm surge) variability along the eastern North Pacific, and to determine principal components (PCs) of anomalous activity. Trends in correlations significantly different from zero were determined throughout this study using a two-sided Student's *t* test linear regression null-hypothesis test at the 95% confidence level [*Hines and Montgomery*, 1980].

2.1. Spatial Tide Gauge Distribution

Here we employ a network of tide gauges from Yukatat, AK to San Diego, CA (Figure 1a) of various record lengths (Table 1) to characterize storm surge variability, primarily since about 1950 when more tide gauge stations were in operation. The large latitudinal distribution of tide gauges employed provides a network that is sensitive to changes in both the intensity and location of eastern North Pacific winter storm landfalls.

Coastal storm surge variation is dominated by relatively local storminess, with very low SLP (i.e., intense storminess) near tide gauge stations producing high storm surge levels. Extreme storm surge levels occur at coastal locations nearest landfall, shown for the 5 January 2008 extreme storm event that impacted the Cascadia and British Columbia (BC) coasts. The north-south pattern of nontide variability in Figure 1b shows the strong influence of SLP on storm surge levels, i.e., the strongest surge is near the deep SLP low north of Vancouver Island in contrast to low surge along the coast south of Cape Mendocino (CM) where higher SLP during this event is observed. Although dominated by the inverse barometer effect, local winds, currents, and coastline geometry (e.g., bays and harbors) can also affect surge levels. However, the systematic variation of storm surge for the storm events shown in Figure 1b suggests that shelf configuration in this study region is not a dominant factor.

Prefrontal winds likely contribute to the highest surge levels for the 5 January storm recorded at Tofino, Vancouver Island (TOF), resulting in the highest surge not being exactly coincident with the location of the deepest low. In contrast to the SLP pattern during the 5 January storm, higher surge levels were observed south of Cape Mendocino during 25–28 January when a moderate storm system impacted the central California coast (supporting information Figure S1). Lower SLP south of Cape Mendocino relative to the north causes higher surge in the south. This linkage of surge to SLP indicates that approximate storm landfall locations can be differentiated from surge variability along the Pacific coast of North America.

Over land, a primary indicator of storminess is precipitation, which can be strongly influenced by topography and related orographic effects. Because of spatial variation and because estimates of storminess using storm surge and rainfall parameters are dependent on both their intensity and duration, each of these measures of storminess has somewhat different temporal and amplitude characteristics. However, along eastern North Pacific coasts, atmospheric rivers produce heavy rainfall at northern California and Cascadia coastal regions [*Ralph et al*., 2013; *Dettinger*, 2011]. Strong storm surge is anticipated when these intense low-pressure systems make landfall, with the linkage to rainfall compounding the impact of coincident surge and high waves on sea cliffs that are more prone to fail when saturated, particularly when both high surge and high waves occur near high tide.

2.2. Long-Term Variability

The variability of positive nontide (storm surge) levels with latitude is shown in Figure 2. In an effort to characterize storm surge variability, comparisons were made over different time periods using different thresholds. As high surge is critical for assessing potential coastal impacts, winter (December–February) means of surge levels exceeding the 90th percentile nontide level for all winter observations were examined at stations with long records (Figure 2a). The 90th percentile threshold level for all winter data at each station was chosen so that variability could be assessed in nearly all winters, giving continuous time series. These show substantial interannual variability and exhibit no statistically significant trends since 1935. An increase in nontide levels from south-to-north is observed, with three distinctly different regimes indicated: (i) the high-energy region north of Cape Mendocino, (ii) along the central California coast southward from Cape Mendocino to Point Conception, and (iii) south of Point Conception (station distribution by region shown in Table 1).

The Cape Mendocino demarcation is further demonstrated by latitudinal variability of mean winter nontide levels since the mid-1970s (Figure 2b) that spans the satellite era during which the apparent acceleration of global sea level rise occurred [*Cazenave and Nerem*, 2004; *Bromirski et al*., 2011] when more tide gauge

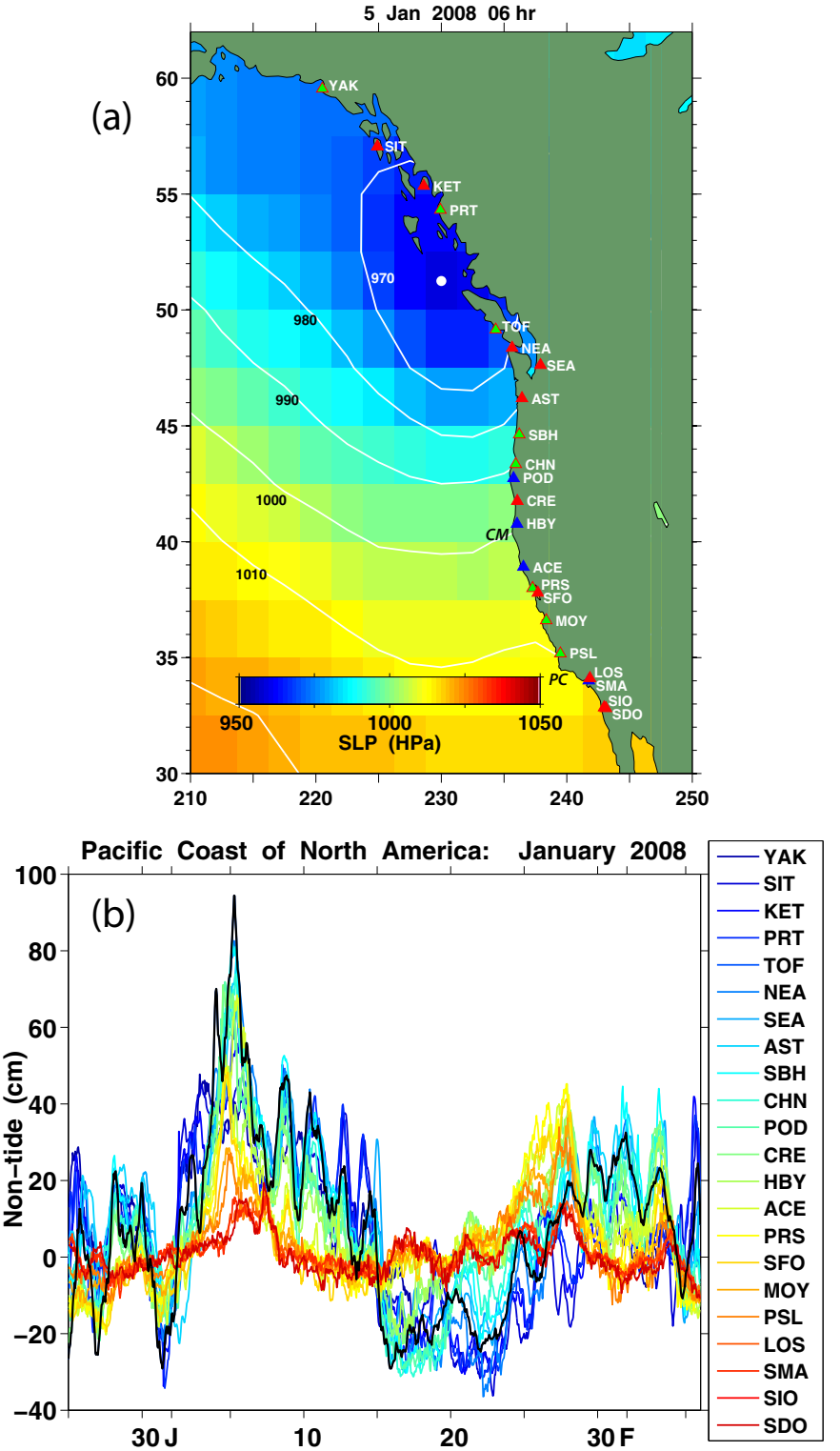

Figure 1. (a) Sea level pressure (SLP) snapshot for an extreme storm event during 5 January 2008. Lowest SLP is 960 hPa (white dot). Locations of tide gauge stations studied are indicated by triangles, with record start dates after 1990 (blue), prior to 1985 but after 1950 (green), and long-duration stations beginning prior to 1950 (red) (see Table 1 for start years and locations). (b) Nontide (storm surge) levels at all stations shown in (a) from 25 December 2007 to 5 February 2008, color-coded north-south blue-red, respectively. The highest surge levels for the 5 January event were at Tofino, Vancouver Island (TOF, black curve overlaid) near the deepest SLP low. Locations of Cape Mendocino (*CM*, 40.4°N, 124.4°W) and Point Conception (*PC*, 34.4°N, 120.5°W) are indicated.

Table 1. Tide Gauge Station Locations and Record Start, All Available Data Through 2014

Location	Station ID	Latitude	Longitude	Start Year
Region 1				
Yakutat	YAK	59.547	−139.735	1961
Sitka	SIT	57.052	−135.3417	1945
Ketchikan	KET	55.353	−131.659	1918
Prince Rupert	PRT	54.317	−130.333	1963
Tofino	TOF	49.150	−125.917	1963
Neah Bay	NEA	48.365	−124.611	1934
Seattle	SEA	47.622	−122.350	1901
Astoria	AST	46.188	−123.821	1925
South Beach	SBH	44.625	−124.0417	1967
Charleston	CHN	43.345	−124.3217	1978
Port Orford	POD	42.738	−124.498	1996
Crescent City	CRE	41.754	−124.198	1933
North Spit, Humboldt Bay	HBY	40.767	−124.217	1993
Region 2				
Arena Cove	ACE	38.913	−123.708	1996
Point Reyes	PRS	37.997	−122.975	1975
San Francisco	SFO	37.793	−122.555	1854
Monterey	MOY	36.605	−121.8867	1973
Port San Luis	PSL	35.177	−120.760	1983
Region 3				
Los Angeles	LOS	34.112	−118.411	1923
Santa Monica	SMA	34.008	−118.500	1995
La Jolla	SIO	32.847	−117.273	1924
San Diego	SDO	32.815	−117.136	1906

stations were in operation. Although the high interannual variability results in only weakly significant trends (confidence levels generally only at about 75% at best), the general pattern indicated by least squares trends shows downward trends south of Cape Mendocino and upward trends north of Cape Mendocino, suggesting a relatively recent general northward shift in storm track anticipated under global warming [*Lu et al.*, 2007; *Frierson et al.*, 2007]. However, trends for the northernmost stations (Yakutat, Sitka, and Ketchikan, AK (YAK, SIT, and KET, respectively); locations given in Figure 1, Table 1) in Figure 2b are downward, suggesting a slightly southward tendency in the dominant storm track that results in a concentration of storm activity along the British Columbia coast.

Consistent with Figures 2a and 2b, winter extreme surge levels are higher in the north, with the peak in extreme surge located along the Cascadia/Vancouver/BC coasts (Figure 2c) that levels off and then tends to decrease somewhat going farther north, in qualitative agreement with the pattern of variability for nontidal residual water levels found by *Menéndez and Woodworth* [2010]. These show that extreme surge levels along the Cascadia coast are about a factor of three greater than Southern California. Seattle (SEA), Astoria (AST), and other stations that have somewhat anomalously low levels are inland from the coast and/or shielded by geographic features. Some of the differences shown result from different record lengths examined. Comparison of winter extremes pre-mid-1970s and post-mid-1970s North Pacific regime shift, which is associated with a deepening of the Aleutian Low and warmer SST along the U.S. West coast [*Miller et al.*, 1994], shows only minor differences, consistent with the lack of significant trends in Figures 2a and 2b. Similar variability shown in Figure 2 is exhibited for other threshold levels not shown. These comparisons indicate that the variability of winter coastal storm intensity has generally not changed appreciably since 1935.

2.3. El Niño/La Niña Winters

There are significant differences in the character and spatial and temporal distribution of storm surge activity levels during ENSO episodes (Figure 3). During El Niños when storm tracks are typically more southerly as a result of the southeastward shift of the Aleutian Low [*Trenberth and Hurrell*, 1994], there is a greater tendency for storm surge levels at more southern locations to be higher than at locations to the north. This is exemplified by consistently higher levels at southern stations (Figure 3a, red lines) than at San Francisco (SFO) during the first half of January 1983, consistent with higher storm activity along the southern California coast during this period. However, reflecting the complexity of broad-scale atmospheric circulation patterns, high surge levels also occur in the Gulf of Alaska during ENSO, consistent with the distribution of extreme surge levels shown in Figure 2.

Indicative of changing intrawinter atmospheric patterns, higher surge levels at SFO in the latter half of January and much of February 1983 suggest that the primary storm landfall location shifted north, although significant surge levels were also attained in southern California. Significantly higher surge levels at SFO and farther north during the 1997–1998 El Niño compared with 1982–1983 indicates that the storm tracks were significantly farther north during this ENSO warm phase. This pattern repeated in the recent 2015–2016 El Niño winter. Earlier and lower than average winter peak high tides also decreased chances for coastal erosion, flooding, and damage in the north and south [*Flick*, 2016]. The more northern surge activity during the 1998–1999 La Niña is characterized by lower activity at SFO and locations to the south (Figure 3c). The strong variability both between and within ENSO episodes highlights the difficulty of anticipating extreme

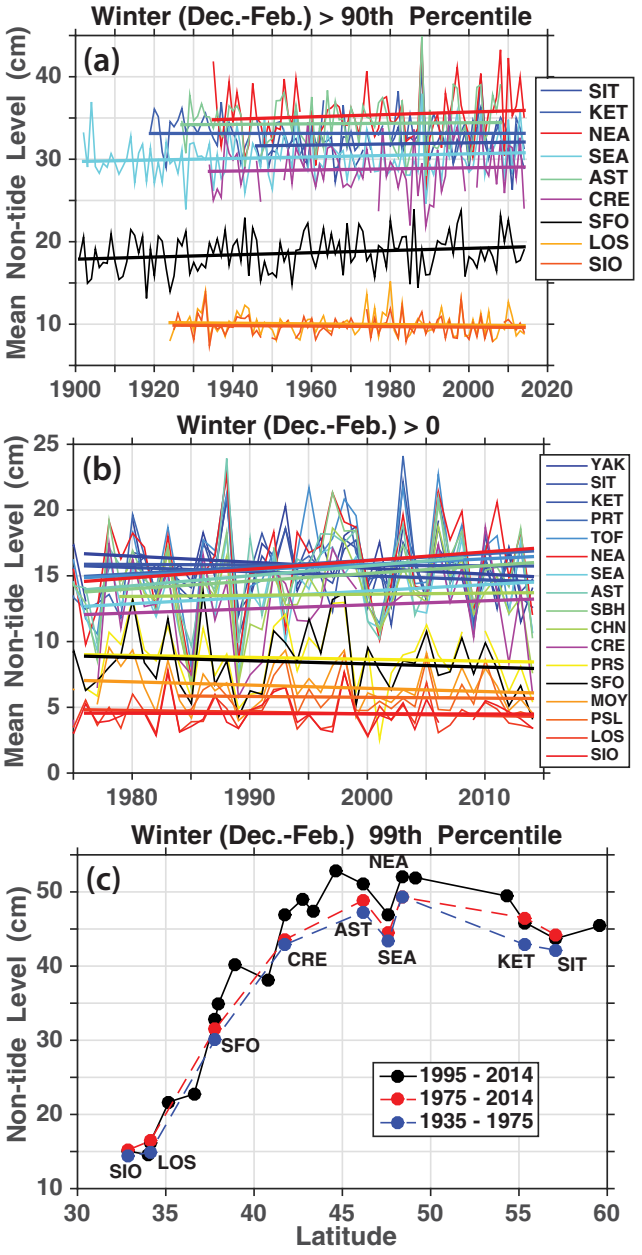

Figure 2. (a) Long-term storm surge variability determined from the mean of all winter (December–February) nontide levels >90th percentile level at each station whose start date is prior to 1950. (b) Mean of all positive winter nontide measurements over the 1975–2014 epoch at each station whose record starts prior to 1980. (c) Winter nontide 99th percentile levels for all available data for the time periods indicated for all stations in Table 1 (black), and for those stations whose records begin prior to 1950 for pre-1975 and post-1975 epochs (red and blue, respectively, labeled). Neah Bay (NEA) pre-1975 and post-1975 levels overlap.

winter synoptic variability of storm surge along the Pacific coast, and emphasizes the high degree of interannual and intrawinter storm surge variability along the Pacific coast of North America.

3. Spatial Patterns

The high degree of winter storm surge variability along the Pacific coast motivates statistical comparison using empirical orthogonal function (EOF) principal component analyses. EOFs were computed for nontide residuals at selected tide gauge stations with nearly complete records, with each record normalized to unit variance to minimize the dominance of the higher amplitude surge levels at the northern stations. To assess whether changes is storm surge spatial patterns have changed over time, EOFs were computed separately for the pre-mid-1970s regime shift 1948–1975 epoch and the satellite era 1983–2014 epoch (Figures 4a and 4e, respectively). These show effectively the same spatial patterns, with small differences attributable to the higher station density during the latter epoch. This is confirmed by the strong similarity of the EOF weighting pattern for the 1983–2014 epoch using the same station network as in Figure 4a, shown in supporting information Figure S2a, and similar nontide PC versus SLP correlation patterns (supporting information Figure S3). The mode 1–3 winter EOFs for the six longest records that extend to 1935 (Table 1) exhibit very similar patterns, over the full record and regardless of which 20 year epoch is analyzed (supporting information Figure S2). The similarity of EOF weightings over the 1935–1948 epoch to those of all other subsequent epochs examined indicates a consistency of decadal storm surge variability that extends at least from about 1935 to the present.

3.1. Spatial Storm Surge Patterns and SLP Associations

The dominant region of storm surge activity associated with each EOF mode can be assessed by correlation of associated principal components with SLP anomalies across the North Pacific basin (Figure 4), determined from the difference of the reanalysis SLP and the long-term climatological mean at each grid point. As would by anticipated by the similarity in the EOF structures, the correlation patterns are also very similar.

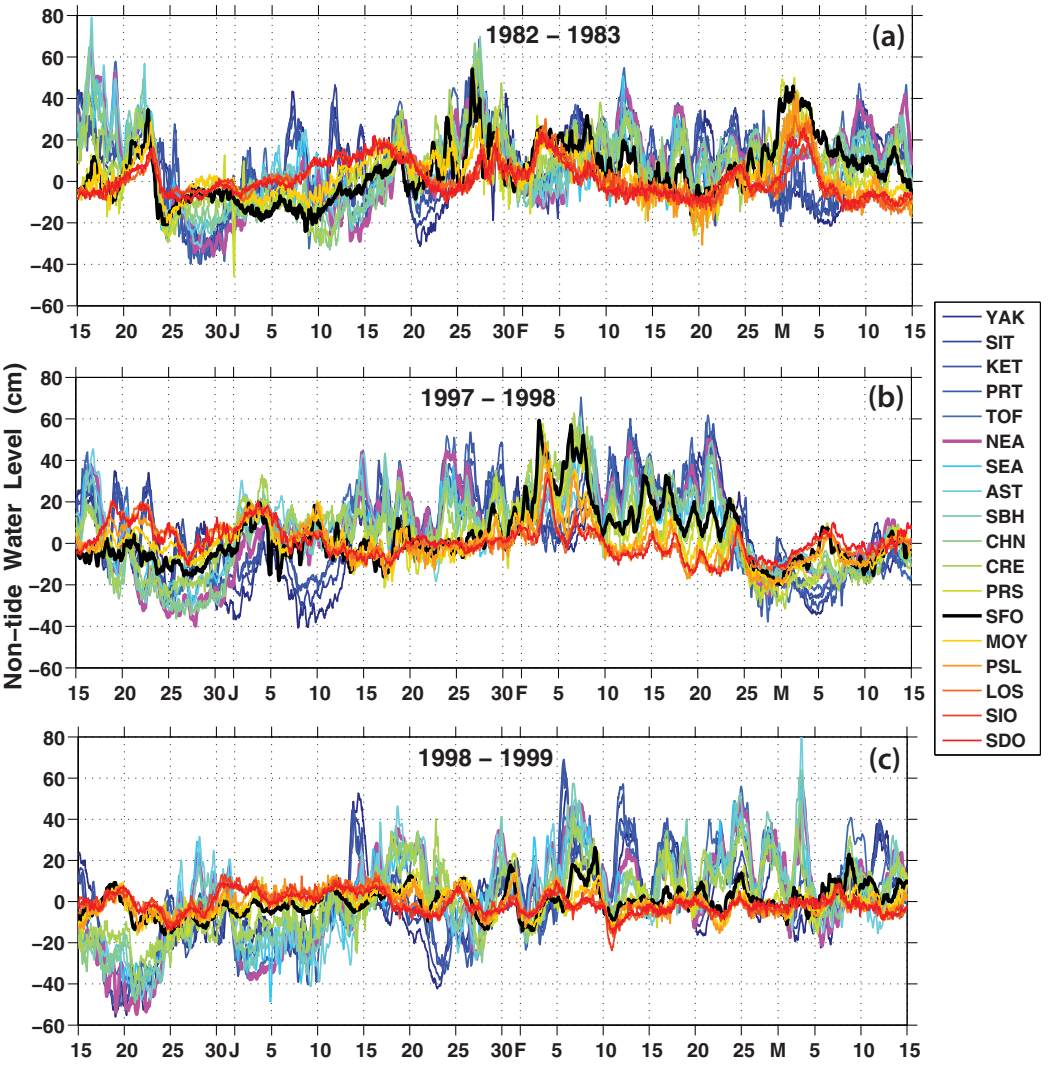

Figure 3. Nontide (storm surge) levels along the Pacific coast of North America during the 1982–1983 and 1997–1998 great El Niños, with the 1998–1999 strong La Niña included for comparison. Coastal stations are color-coded north-to-south (blue to red), with the Neah Bay (NEA, thick magenta) and San Francisco (SFO, thick black) stations identified to help differentiate the dominant regional locations of coastal storm surge activity (see Figure 1 and Table 1 for locations).

The minor differences in *R* spatial patterns between the two epochs can be explained by the inclusion of ten additional stations during the latter epoch.

The mode 1 high *R* (correlation) patterns along the Cascadia/BC coast in Figures 4b and 4f represent the region where typically high storm-forced sea levels occur, associated with the dominant North Pacific storm track landfall location that is strongly influenced by the strength and position of the Aleutian Low [*Hoskins and Hodges*, 2002] The location of high positive correlations for mode 2 (Figures 4c and 4g) is consistent with the generally enhanced influence of El Niño along the California coast, as well as fluctuating atmospheric patterns that affect storm landfall locations. This is evidenced by the storm surge variability shown in Figure 3, which typically results in increased storm activity and precipitation in California [*Bromirski et al.*, 2003].

The mode 3 patterns (Figures 4d and 4h) represent conditions associated with the well-known "blocking high" that results in reduced rainfall in California. As suggested by the interannual variability shown in Figures 2 and 3, these patterns occur for at least some of the time during each winter, with their persistence characterized by the amount of variance the modes explain. However, the similarity of the *R* patterns for the two epochs indicates that the general distribution of storm surge extremes along the Pacific coast of

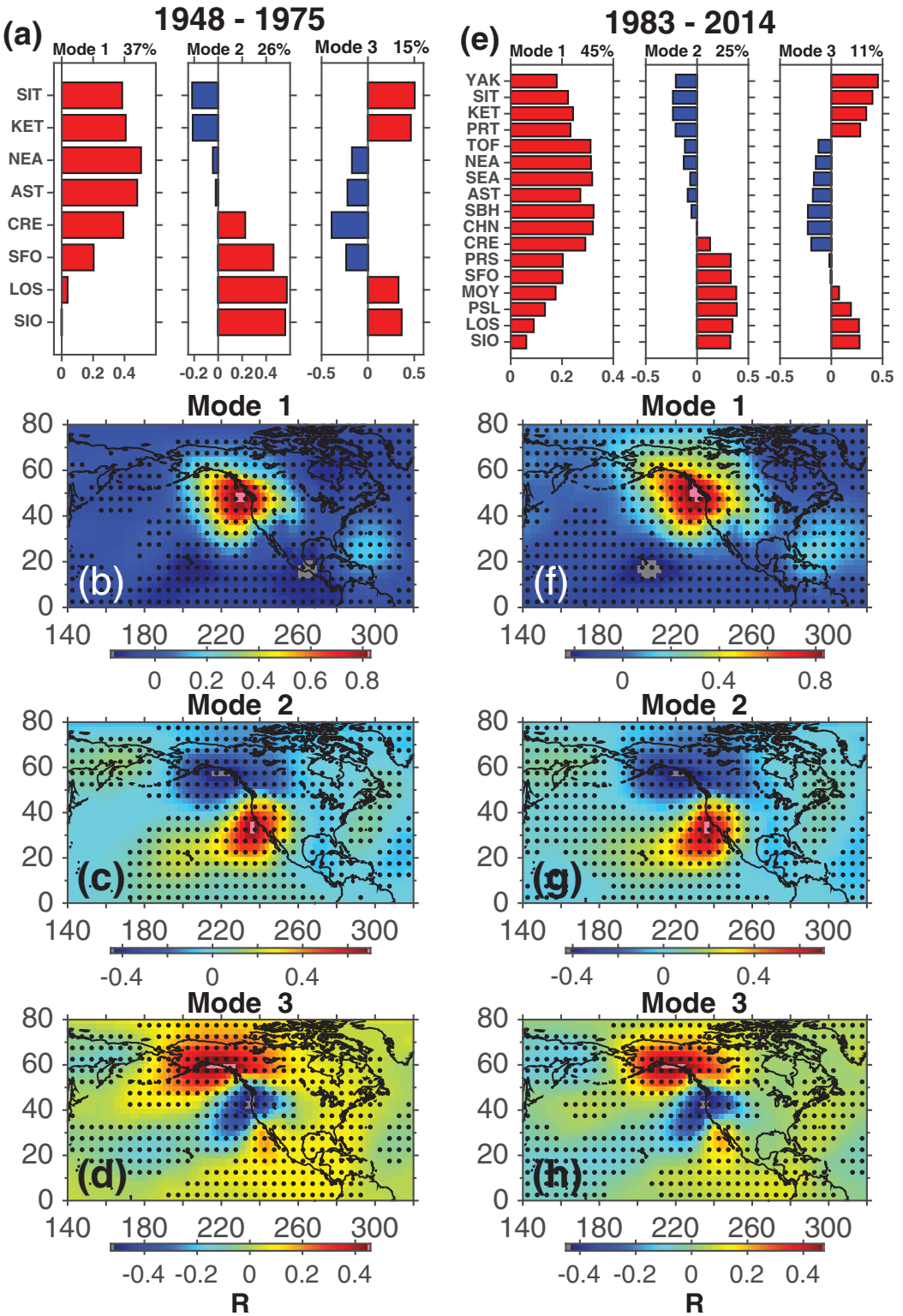

Figure 4. (a) Empirical orthogonal functions (EOFs) of hourly nontide (storm surge) variability over long-duration records during winter (December–February) over the 1948–1975 and 1983–2014 epochs for modes 1–3 from an eight-station tide gauge network along the Pacific coast of North America from La Jolla, CA (SIO) to Sitka, AK (SIT) (see Figure 1 and Table 1 for locations). The percent of variance explained for each mode is given in the subplot title. (b–d) Correlation coefficients (*R*) between respective principal component time series for modes 1–3 in Figure 4a with 6-hourly sea level pressure (SLP) anomalies during respective winter months (December–February). Positive (negative) *R* is associated with negative (positive) SLP anomalies. Regions where *p*-values are less than 0.05 are indicated by black dots. (e–h) Same as Figures 4a–4d except for the 1983–2014 epoch. *R* plots were auto-scaled to emphasize the similarity of correlation patterns between the two epochs.

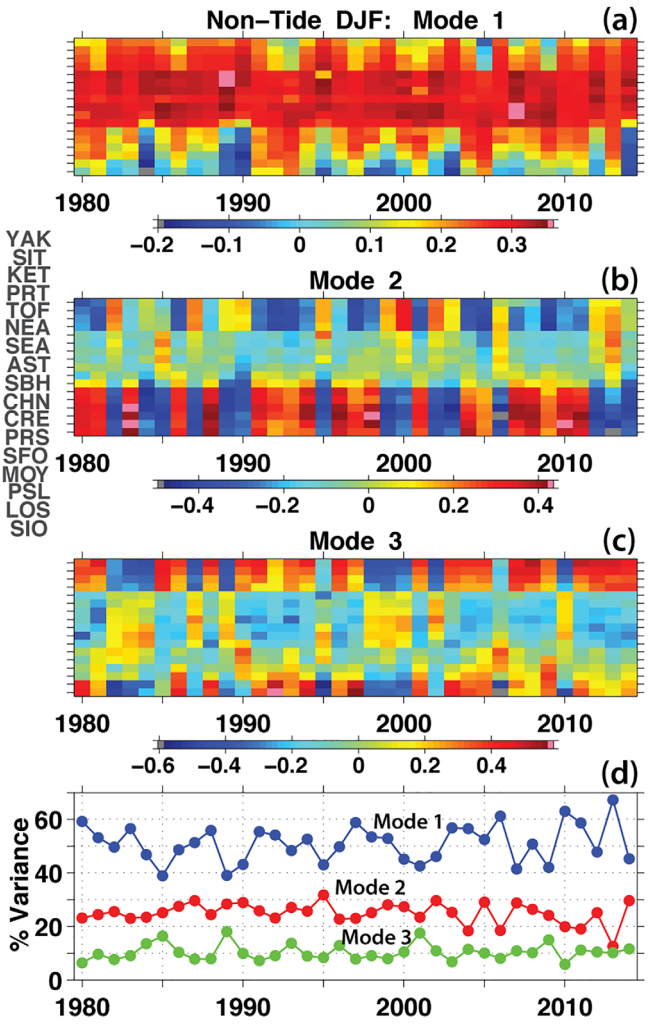

Figure 5. (a–c) Winter (December–February) empirical orthogonal function (EOF) weightings for modes 1–3 of nontide water levels at tide gauges along the Pacific coast of North America from La Jolla, CA (SIO, south, bottom) to Yakutat, AK (YAK, north, top) during each winter (December–February) from 1980 to 2014. Station labels at left apply to Figures 5a–5c. (d) Variance explained by each mode in Figures 5a–5c.

North America has been largely unaffected by climate change, and suggests that multiyear broad-scale patterns of atmospheric variability have not changed appreciably over the past 70 years.

3.2. Interannual Winter Variation

To investigate the interannual variability of the spatial patterns determined by the relatively long-record nontide EOF principal component SLP correlations in Figure 4e, the EOF structures for modes 1–3 were determined for each winter period individually from 1980 to 2014 (Figure 5). These structures are, on average, consistent with both the EOF long-term structures and the SLP anomaly correlation patterns shown in Figure 4, with the latitudinal variability showing the persistent influence of these modes. While substantial interannual variability is observed, both the location of the highest weightings in Figure 5a and the consistently significantly higher variance explained by mode 1 (Figure 5d) confirm that the region of dominant storm surge activity is north of Cape Mendocino, extending from about Crescent City (CRE) to Tofino (TFO), and that activity in this region is generally dominant even in El Niño years. The highest weightings for mode 2 (Figure 5b) occur in the south during the strong 1983, 1998, and 2010 El Niño winters, suggesting some association with ENSO. The mode 3 pattern (Figure 5c) typically shows low storm surge weightings in the region associated with low correlation of nontide PC3 with SLP in Figure 4h, interpreted to be indicative of low storm activity resulting from blocking high SLP in that region.

3.3. Association With Broad-Scale Climate Patterns

For storm impacts preparedness, it is useful for coastal managers to be able to anticipate winter storm activity levels. The utility of climate indices to anticipate patterns of storm surge variability was investigated by correlating nontide principal components with climate indices associated with broad-scale atmospheric variability, including the multivariate ENSO Index (MEI) [*Wolter and Timlin*, 1998], the North Pacific pattern (NP) [*Trenberth and Hurrell*, 1994] associated with the strength of the Aleutian Low, the Pacific North America pattern (PNA) [*Wallace and Gutzler*, 1981], and the Northern Oscillation Index (NOI) [*Schwing et al.*, 2002]. To compare with these monthly indices, principal components (PCs) for modes 1–3 were determined for nontide monthly means at the long-durations stations employed in Figure 4a. While correlations of monthly anomalies are not expected to accurately represent the synoptic variability shown in Figure 3, monthly correlations can nevertheless be useful to identify whether there is a dominant mode of variability that influences the storm surge patterns observed.

Table 2. Correlation Coefficients, *R*, of Principal Components (PCs) of Monthly Mean Anomalous Nontide Sea Level (Storm Surge) With Monthly Climate Indices During Winter Months (December–February) Over the 1948–2014 Epoch[a]

Mode	MEI	*p*	PNA	*p*	NOI	*p*	−NP	*p*	−SLP	*Hs*
1	**0.50**	0.000	**0.44**	0.000	**−0.49**	0.000	**0.45**	0.000	**0.82**	**0.54**
2	0.21	0.103	0.01	0.932	**−0.40**	0.001	0.12	0.355	**0.82**	**0.27**
3	**0.26**	0.044	**0.37**	0.003	**0.27**	0.030	**0.28**	0.003	**0.78**	**0.33**

[a]Correlations with *p*-values < 0.05 (in bold) are considered significant. Correlations with −SOI gives *R* similar to MEI. Included are correlations between PCs of anomalous 6 h sampled SLP (at nearest grid points, normalized to unit variance) and wave *Hs* with nontide PCs associated with EOFs shown in Figure 4e, with *p*-values < 0.001 for all modes.

Nontide PC1 is significantly well correlated with North Pacific atmospheric circulation (SLP and geopotential height) indices NP, PNA, and NOI, respectively, and with the MEI ENSO index (shown in supporting information Table S2), with correlation coefficients, *R*, near 0.5 for all atmospheric derived indices, consistent with typical large-scale SLP patterns during winter months [*Bromirski et al*., 2005]. None of these climate modes dominates over decadal time scales, although the sparse long-record station distribution could be a factor. The sea surface temperature (SST) derived PDO is uncorrelated with the first three PCs of nontide variability. This suggests that the longer period decadal variability associated with the PDO (that imposes a strong decadal signal in mean RSL [*Bromirski et al*., 2011] and is associated with decadal variability of waves [*Bromirski et al*., 2013]) does not reflect the much shorter period tide gauge-measured synoptic variability of storm surge, i.e., Pacific basin SST variability and synoptic storminess along the eastern boundary are apparently not closely related.

PC2 represents the north-south mode and is well balanced, and is consequently not strongly influenced by any particular mode of climate variability with the exception of NOI, which has a northeast Pacific atmospheric pressure association that influences both storminess along the Pacific coast and associated precipitation in California [*Costa-Cabral et al*., 2016]. The significant negative correlation of nontide PC2 with NOI emphasizes the importance of the eastern Pacific blocking high on weather patterns and rainfall along the U.S. Pacific northwest, and of precipitation patterns over northern California [*Costa-Cabral et al*., 2016]. Together with PC1 correlations, weaker but significant correlations of these indices with PC3 suggest that each of the climate modes of variability affects the pattern and intensity of storm surge along the Pacific coast, with no dominant climate factor controlling.

Monthly mean nontide PCs are uncorrelated with monthly SLP anomaly PCs, indicating that comparisons on monthly time scales do not well characterize storm surge synoptic variability (and patterns). The monthly climate indices identify broad-scale climate patterns that include remote components not directly related to local SLP-forced storm surge events. To demonstrate the association of local synoptic SLP variability with storm surge, nontide principal component time series were correlated with principal components of 6 h sampled anomalous SLP extracted at the grid points closest to each of the 17-station network employed in Figure 4e. The high correlation between synoptic-scale PCs of nontide variability and anomalous SLP shown in Table 2 confirms the close association of coastal SLP variability and storm surge.

3.4. Great El Niño SLP Patterns

The 1982–1983 and 1997–1998 great El Niños resulted in severe impacts along the California and Cascadia coasts [*Griggs and Brown*, 1998; *Storlazzi and Griggs*, 2000; *Flick*, 1998, 2016]. Most measures of El Niño strength (e.g., NINO3.4 [*Kumar and Hoerling*, 2003], MEI, and NP) suggest that the strengths of these events are comparable. Although correlations of the dominant nontide mode 1 PC with these climate indices give similar *R*-values (Table 2), these long-term monthly correlations do not provide sufficient information to adequately explain the spatial and temporal variability of synoptic surge levels along the Pacific coast shown in Figures 3a and 3b, or for the 2015–2016 great El Niño in Figure 6a. The dominance of surge activity north of Cape Mendocino (CM) is evident. Qualitative comparisons of nontide levels during the 1982–1983, 1997–1998 (Figures 3a and 3b, respectively), and 2015–2016 (Figure 6a) El Niños suggest that surge activity was higher south of CM during the earlier events (evidenced by the occurrence of surge levels $>$40 cm at SFO, thick black line in Figures 3a and 3b) than during 2015–2016, suggesting a northward shift in landfalls of strong storms.

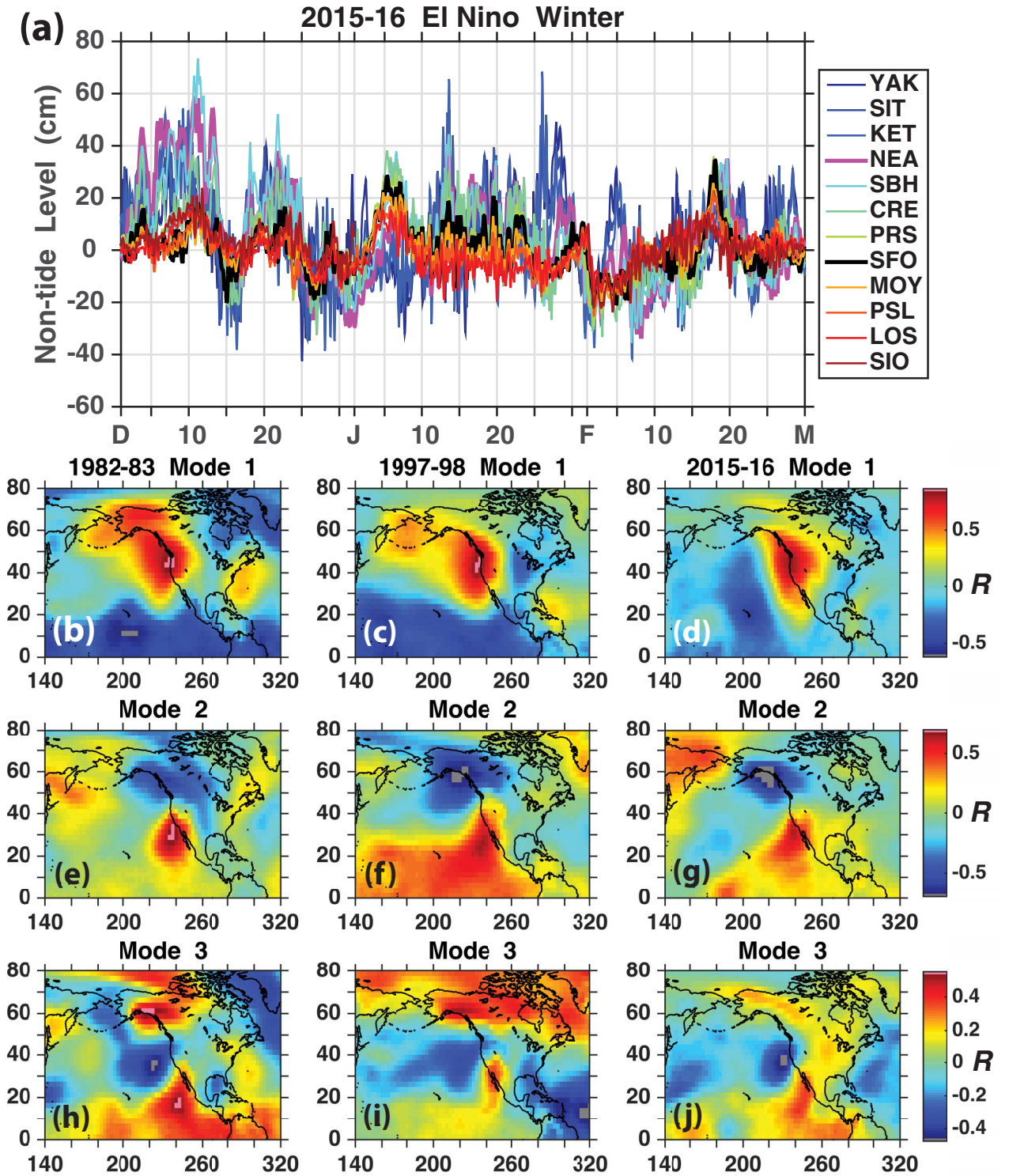

Figure 6. (a) Nontide (storm surge) levels along the Pacific coast of North America during winter months (December–February) of the 2015–2016 great El Niño. (b–j) Correlation coefficient, *R*, patterns over the North Pacific determined between nontide mode 1–3 principal components (PCs) with anomalous SLP. PCs were obtained for nontide data at the stations shown in Figure 6a for great El Niños during (left column) 1982–1983 (percent variance (σ) explained for modes 1–3: $\sigma_1 = 50.0$, $\sigma_2 = 28.6$, $\sigma_3 = 11.3$), (middle column) 1997–1998 ($\sigma_1 = 45.4$, $\sigma_2 = 32.4$, $\sigma_3 = 10.7$), and (right column) 2015–2016 ($\sigma_1 = 53.2$, $\sigma_2 = 21.1$, $\sigma_3 = 8.2$). Correlation patterns for each mode were scaled separately for the three El Niños using the *R*-scalings shown on the right.

To investigate the differences between these El Niño episodes, nontide PCs for December–February winter months for the three El Niños were determined separately using the stations shown in Figure 6a, with PCs 1–3 correlated with SLP anomalies across the North Pacific basin as in Figure 4 allowing for qualitative

comparisons between these events. Positive correlations are associated with low SLP (heightened storminess), while negative correlations are associated with high SLP. The highest positive correlations of PC1 with SLP for these great El Niños occur along the same stretch of the Cascadia/BC coast (Figures 6a–6d) as in Figure 4, likely strongly influenced by the well-known intensification of the Aleutian Low during strong El Niños [*Trenberth and Hurrell*, 1994], which is also the dominant pattern during most, if not all, non-El Niño winters (Figures 4 and 5a).

High *R* extending over Alaska and the Bering Sea during the 1982–1983 El Niño (Figure 6b) further demonstrates the linkage of strong storm systems (low SLP) associated with an intensified Aleutian Low. Progressively decreasing *R* over Alaska and the Bering Sea during the latter El Niño events (Figures 6c and 6d) suggests that the influence of the Aleutian Low during these extreme El Niños apparently has diminished over time. However, as Figures 6a–6d show, the Cascadia/BC coast and northeastern Gulf of Alaska were nevertheless subjected to intense storm activity during these great El Niños.

High *R* south of southern California near 240°E for modes 2 and 3 during the 1982–1983 El Niño (Figures 6e and 6h) suggests a stronger influence of tropical eastern Pacific El Niño conditions on storm patterns during the 1982–1983 winter, which produced greater coastal impacts than the 1997–1998 El Niño [*Storlazzi et al*., 2000]. The apparent enhanced influence of storm systems approaching the coast from the eastern Pacific tropics is consistent with the higher rainfall and greater coastal damage experienced across southern California during the 1982–1983 El Niño compared with 2015–2016.

The lower positive *R* over the northern Gulf of Alaska combined with the stronger negative *R* (high SLP) nearer the coast during 2015–2016 (Figure 6j) indicates a change in the mode 3 dipole from 1982 to 1983 (Figure 6h), together resulting in lower precipitation over the Sierra-Nevada Mountains during 2015–2016 than in the two previous great El Niños. Furthermore, generally low or negative correlations of PC3 with SLP during 2015–2016 along the entire eastern Pacific coast and the proximity of the negative dipole to the coast (Figure 6j) are consistent with a greater influence of the mode 3 blocking high pattern on eastern North Pacific storm patterns than previously occurred.

4. Coastal Impacts

Surface gravity waves provide much of the energy that drives physical processes along coasts. Coastal storm damage is linked to strong surge and high waves arriving near high tide [*Flick and Cayan*, 1984]. While the tide and mean RSL are critical factors, they are independent of each other and independent of storm surge and waves. However, because strong storms produce both high waves and high surge near landfall locations, these commonly occur coincidentally [*Cayan et al*., 2008; *Bromirski et al*., 2012]. The strong association of heightened wave activity and storminess with broad-scale atmospheric circulation patterns [*Bromirski et al*., 2003, 2005] suggests that extremes in both storm surge and waves can commonly occur.

4.1. Coastal Wave Variability

To establish the strength of the linkage between high surge and high waves, representative coastal wave activity was first determined from WW3 wave model *Hs* as the average of *Hs* at five grid points centered at the nearest grid node 3° west of the 17-location tide gauge network that determined nontide spatial structures in Figure 4e. The spatial variability of near-coastal *Hs* was determined from anomalous *Hs* formed by subtracting the climatological mean *Hs* over the 1980–2008 time period at each location. Principal components were obtained for EOF modes 1–3 of anomalous *Hs* normalized to unit variance, minimizing the dominance of wave activity north of Cape Mendocino [*Bromirski et al*., 2005, 2012, 2013].

The first three EOF modes of wave variability for the 17-location model *Hs* estimates are shown in Figure 7a. The similarity of EOF patterns for storm surge in Figures 4e and *Hs* in Figure 7a indicates a common spatial variability. Correlation of nontide PC1 for the 17-station network with the 6-hourly WW3 model *Hs* over the northeast Pacific from 1980 to 2008 produces an *R* pattern (Figure 7b) that strongly resembles the *R* pattern between the same PC1 and SLP in Figure 4f, suggesting that coincident high waves and high storm surge are common along the Cascadia/BC coast. Nontide PC1 and near-coastal wave *Hs* PC1 are well correlated (Table 2), confirming the close association of surge and waves along the Pacific coast. As storm surge is dominated by local storm activity, small dissimilarities between Figures 4f and 7b reflect the occurrence of swell generated under distant storms in the dominant wave generation region [*Bromirski et al*., 2013] that

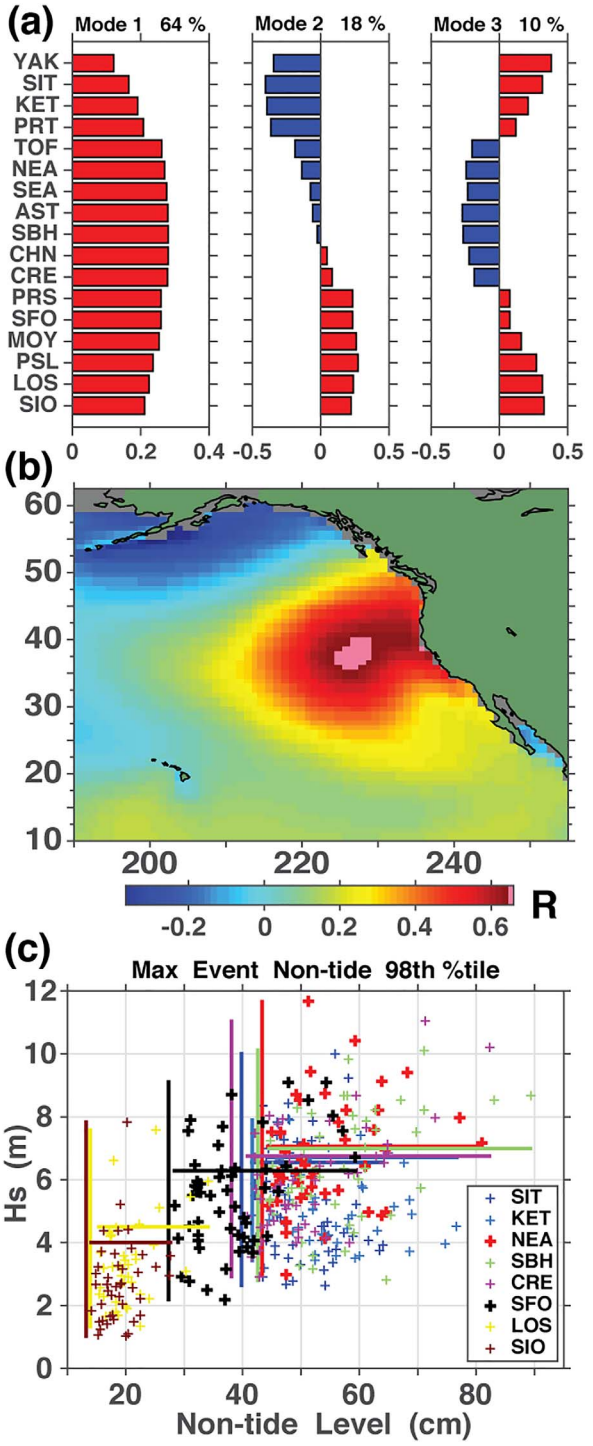

Figure 7. (a) Structure of the first three EOF modes of WW3 model anomalous *Hs* computed at 6 h intervals during winter (December–February) determined at the nearest grid nodes 3°W of the tide gauge stations studied in Figures 4 and 5 (compare with the nontide EOF spatial patterns in Figure 4). (b) Correlation on nontide PC1 (associated with EOF mode 1 in Figure 4e) with WW3 wave model anomalous *Hs* across the northeast Pacific. (c) Extreme storm surge (nontide) event maximum levels and associated maximum wave *Hs* during each event at selected locations along the North American Pacific coast during 1980–2008 winters (December–February). The ranges of peak surge amplitudes for all extreme winter events identified are indicated by horizontal lines, while vertical lines give the *Hs* range.

propagate southward along the coast, which are unrelated to local coastal storm activity. Thus, high waves can be observed at coastal locations when no local storm activity occurs, and results in lower correlations between surge and wave PC2 and PC3, in contrast to correlations between surge and SLP PC2 and PC3 (Table 2) that are locally connected.

4.2. Extreme Storm Surge Events (SS_E) and High Waves

Here extreme storm surge events (SS_E) are identified by hourly nontide levels continuously exceeding a prescribed threshold for at least 6 consecutive hours. These constraints on event identification allow characterization of changes in the incidence and spatial variability of strong storm surge events that generally cause the greatest coastal and societal impacts. The 98th percentile threshold level was determined for all nontide data during December–February over the 29 winter seasons from 1980 to 2008 (Table 3), spanning the satellite era. This threshold was selected so that one or two extreme events, on average, would be identified in each year. For each identified event, the maximum significant wave height, *Hs*, during the event was determined from the wave model data.

The maximum SS_E follow the pattern of variability shown in Figure 2, with both extreme SS_E and *Hs* attaining their highest amplitudes along the Oregon/Washington/BC coasts (Figure 7c, Table 3). Although transformation of deep-water waves to the coast introduces some uncertainty at particular coastal locations with respect to the wave threshold, high offshore waves are typically associated with high waves at the coast everywhere except in parts of southern California that are shielded by Point Conception and are affected by variable coastal orientation and island blocking.

In general, not considering farthest north and farthest south stations, extreme storm surge and extreme waves commonly occur concurrently about a third of the time (Table 3). This is particularly problematic for the Oregon/Washington/BC coasts, and even as far south as the San Francisco region, where, for example, during the event at SFO that produced the 59 cm peak level, the peak *Hs* during that

Table 3. Common Occurrences of High Nontide And High Waves During the1980–2008 Winters (December–February)[a]

Station ID	# Events	Nontide Threshold (cm)	Max. Nontide (cm)	Median Nontide (cm)	Wave *Hs* Threshold(m)	% Common
YAK	58	41.4	74	53	5.4	10
SIT	62	39.8	64	48	6.6	27
KET	50	41.6	77	54	6.7	10
PRT	47	44.1	80	55	5.9	13
TOF	57	44.6	89	57	7.1	23
NEA	47	43.3	81	51	7.1	40
SEA	66	38.1	74	49	6.1	36
AST	54	42.5	91	55	7.0	44
SBH	49	42.6	89	57	7.0	39
CHN	46	38.6	82	47	6.8	35
CRE	49	38.1	82	49	6.8	29
PRS	48	28.5	59	41	6.3	35
SFO	54	27.3	59	37	6.3	31
MOY	48	20.1	40	27	6.0	29
PSL	37	17.3	49	25	5.6	22
LOS	40	13.9	34	19	4.5	15
SIO	43	13.2	28	19	4.0	12

[a]Extreme storm surge events were identified by nontide levels exceeding the 98th percentile level threshold for at least 6 consecutive hours. Event parameters at each location (for hourly nontide data for all events for all winters) are the maximum nontide and median levels for all extreme events identified at each station. The percent of events when winter *Hs* exceeded the 98th percentile level for all winters at respective stations are given (see Figure 6).

event was about 6.5 m. Notably, many of the wave events during high surge events in Figure 7c that do not exceed the arbitrary 98th percentile *Hs* threshold are still significant. While 4 m waves are somewhat below the 98th percentile threshold used, they can still be significant [*Seymour*, 1996]. Many of the wave heights during the extreme surge events identified at locations north of Point Conception have $Hs > 4$ m and can cause appreciable damage when coincident with extreme surge near high tide. Thus, many of the wave events occurring during extreme surge at SFO and stations farther north can have significant coastal impacts.

The Pacific coast of North America has a mixed-tide regime characterized by two usually unequal daily high tides [*Zetler and* Flick, 1985], with both the diurnal and mean peak-to-trough tide ranges generally increasing from south (SIO, about 3 m) to north (SIT, about 4.5 m). Putting the magnitude of surge levels in perspective, the median extreme SS_E level at SFO is about 25% of the maximum tide height above the mean ($\sim$1.5 m). Significantly, about 75% of the events in Figure 7c have durations greater than 12 h, which ensures that these events will occur during a high tide, although potentially not during the highest diurnal level. If any of these extreme events occur near high tide, there is a strong likelihood that significant coastal erosion, flooding, and damage will occur.

5. Discussion

The importance of rising sea levels on coastal impacts has inspired numerous studies to describe potential increases in extremes associated with climate change and variability [e.g., *Cayan et al*., 2008; *Wahl and Chambers*, 2015; *Barnard et al*., 2015). General extreme value (GEV) modeled nontide residual trends [*Menéndez and Woodworth*, 2010] and global climate model (GCM) derived projections of storm surge and wave activity along the California coast to 2100 [*Bromirski et al*., 2012; *Hemer et al*., 2013; *Graham et al*., 2013; *Erikson et al*., 2015] are in general agreement, showing small or no upward trends along eastern North Pacific coasts. The apparent absence of trends in storm surge and waves in both observation and model studies is somewhat at odds with projected changes in atmospheric circulation patterns due to climate change [*Lu et al*., 2007; *Hu and Fu*, 2007].

The lack of substantial upward trends in either surge or waves is somewhat surprising because changes in the global Hadley circulation under global warming are anticipated to affect atmospheric circulation in the subtropics, and thereby affect storm track activity and eastern Pacific landfalls of the storms. The Hadley circulation is a zonally integrated atmospheric circulation pattern that is thermally driven by rising warm tropical air that then flows poleward. Poleward expansion of the Hadley circulation under global warming is expected to contribute to an increased frequency of midlatitude drought [*Hu and Fu*, 2007]. *Oort and*

Yienger [1996] found a significant correlation between Hadley circulation and El Nino/Southern Oscillation (ENSO) events, although *Hu and Fu* [2007] determined that the poleward expansion of Hadley circulation appears to not be caused by ENSO events.

However, differences between 2015 and 2016 storm surge/SLP correlation patterns shown in Figure 6 may result from the Hadley Cell expansion and possibly related changes in the Walker circulation that can drive atmospheric teleconnections to the North Pacific [*Oort and Yienger*, 1996; *Wallace and Gutzler*, 1981]], affecting storm track and landfall locations along the Pacific coast of North America. But since the Hadley Cell is defined by zonally integrated variables, it is not surprising that the regional effects in the North Pacific vary from year to year, evidenced by the variability shown in Figure 5. Because of the strong interannual variability across the North Pacific and the influence of climate factors other than the Hadley circulation, the Hadley effect on storm track and landfall locations may not be evident even over decadal time periods (Figure 4), but possibly could be most clearly manifested during extreme El Niños.

The greatest coastal damage occurs when events having extreme waves and extreme storm surge occur near high tide. While the chance of the occurrence of high surge and high waves exactly at high tide is small [*Bromirski et al*., 2012], the values in Table 3 provide an estimate of the worst-case scenario if they occurred near high tide. Since both storm surge and tides are superimposed on mean RSL, rising sea levels will aggravate coastal storm damage from wave impacts going forward, with the potential for moderate storms at the end of the century producing impacts equivalent to or greater than the most severe storms during the 1982–1983, 1997–1998, and 2015–2016 great El Niños [*Cayan et al*., 2008].

Since the patterns of storm surge variability are persistent (Figure 4) and there is no significant trend in nontide variability (Figure 2), and generally small trends in near-coastal buoy *Hs* [*Gemmrich et al*., 2011] and hindcast wave model *Hs* [*Graham and Diaz*, 2001; *Bromirski et al*., 2013, *Erikson et al*., 2015], the spatial distribution of the magnitudes of storm surge and waves along the Pacific coast presented in Table 3 are likely representative of those to be expected over the 21st century. This conclusion is supported by GCM derived projections of storm surge and wave activity along the California coast to 2100 [*Cayan et al*., 2008; *Bromirski et al*., 2012; *Hemer et al*., 2013; *Graham et al*., 2013; *Erikson et al*., 2015]. Thus, because surge and coastal waves are not projected to increase substantially, the controlling factor for heightened coastal impacts is rising coastal mean RSL, which can be significantly enhanced on interannual time scales by El Niños and the strength of PDO warm phases.

6. Conclusions

Rising sea level under global warming scenarios will pose significant challenges for coastal infrastructure in the future. Although there is substantial interannual variability, patterns of storm surge variability along the Pacific coast of North America have not changed appreciably on decadal time periods since at least 1948. Storm surge levels generally increase from southern California to Alaska. Patterns of variability and trends of nontide levels indicate that storm intensity along the Pacific coast, on average, has not increased. The highest storm surge (nontide) levels along the Pacific coast occur north of Cape Mendocino along the Cascadia/British Columbia coasts. Extreme storm surge and extreme waves both occur during extreme events about 30% of the time. Correlations of nontide principal components during extreme El Niños with SLP anomalies across the North Pacific show apparently progressive changes in storm surge amplitudes and their spatial and temporal distribution from the 1982–1983 extreme El Niño to the recent 2015–2016 event, with the observed differences possibly related to changes in the Hadley circulation expected under global warming. Because GCM-projected surge levels show no substantial upward trends over the rest of the 21st century, the controlling factor for heightened coastal impacts is rising coastal mean sea level.

Acknowledgments
Support for this study from the California Department of Parks and Recreation, Division of Boating and Waterways grant DPR/C1570002 is gratefully acknowledged. Miller was supported by NSF OCE1419306. We thank David Jay for providing Columbia River flow-corrected Astoria, OR tide gauge data. Tide gauge data were obtained from NOAA National Ocean Service (NOS) Center for Operational Oceanographic Products and Services (Co-Ops) and the University of Hawaii Sea Level Center. NOAA National Centers for Environmental Prediction (NCEP) reanalysis SLP were obtained from the NOAA National Climate Data Center (NCDC). We thank Paul Wittmann and John Helly (hellyj@ucsd.edu) for providing the wave model data used in this study, archived at the San Diego Supercomputer Center. We thank the two anonymous reviewers who helped to improve the paper.

References

Anderson, J. R., and J. R. Gyakum (1989), A diagnostic study of Pacific basin circulation regimes as determined from extratropical cyclone tracks, *Mon. Weather Rev.*, *117*, 2672–2686.

Barnard, P. L., et al. (2015), Coastal vulnerability across the Pacific dominated by El Nino/Southern Oscillation, *Nat. Geosci.*, *8*, 801–807, doi: 10.1038/ngeo2539.

Bromirski, P. D., R. E. Flick, and D. R. Cayan (2003), Storminess variability along the California coast: 1858–2000, *J. Clim.*, *16*(6), 982–993.

Bromirski, P. D., D. R. Cayan, and R. E. Flick (2005), Wave spectral energy variability in the northeast Pacific, *J. Geophys. Res.*, *110*, C03005, doi:10.1029/2004JC002398.
Bromirski, P. D., A. J. Miller, R. E. Flick, and G. Auad (2011), Dynamical suppression of sea level rise along the Pacific coast of North America: Indications for imminent acceleration, *J. Geophys. Res.*, *116*, C07005, doi:10.1029/2010JC006759.
Bromirski, P. D., D. R. Cayan, N. Graham, R. E. Flick, and M. Tyree (2012), *Coastal Flooding-Potential Projections: 2000–2100*, Publ. CEC-500-2012-011, 54 pp., Scripps Inst. of Oceanogr., Calif. Energy Comm., Sacramento, Calif. [Available at ftp://ftp.iod.ucsd.edu/peter/Bromirski_etal_Coastal_Flooding_Potential_PIER_CVAS_2012.pdf.]
Bromirski, P. D., D. R. Cayan, J. Helly, and P. Whittmann (2013), Wave power variability and trends across the North Pacific, *J. Geophys. Res. Oceans*, *118*, 6329–6348, doi:10.1002/2013JC009189.
Cayan, D. R., P. D. Bromirski, K. Hayhoe, M. Tyree, M. D. Dettinger, and R. E. Flick (2008), Climate change projections of sea level extremes along the California coast, *Clim. Change*, *87*, 57–73, doi:10.1007/s10584-007-9376-7.
Cazenave, A., and R. S. Nerem (2004), Present-day sea level change: Observations and causes, *Rev. Geophys.*, *42*, RG3001, doi:10.1029/2003RG000139.
Chang, E. K. M. (2007), Assessing the increasing trend in Northern Hemisphere winter storm track activity using surface ship observations and a statistical storm track model, *J. Clim.*, *20*, 5607–5628.
Chelton, D. B., and R. E. Davis (1982), Monthly mean seal-level variability along the west coast of North America, *J. Phys. Oceanogr.*, *12*, 757–784.
Costa-Cabral, M., J. S. Rath, W. B. Mills, S. B. Roy, P. D. Bromirski, and C. Milesi (2016), Projecting and forecasting winter precipitation extremes and meteorological drought in California using the North Pacific High sea level pressure anomaly, *J. Clim.*, *29*(13), doi:10.1175/JCLI-D-0525.1.
Dettinger, M. (2011), Climate change, atmospheric rivers, and floods in California: A multimodel analysis of storm frequency and magnitude changes, *J. Am. Water Res. Assoc.*, *47*(3), 514–523, doi:10.1111/j.1752-1688.211.00546.x.
Erikson, L. H., C. A. Hegermiller, P. L. Barnard, P. Ruggiero, and M. van Ormondt (2015), Projected wave conditions in the Eastern North Pacific under the influence of two CMIP5 climate scenarios, *Ocean Modell.*, *96*, 171–185.
Flick, R. E. (1998), Comparison of California tides, storm surges, and sea level during the El Niño winters of 1982-83 and 1997-98, *Shore Beach*, *66*, 7–11.
Flick, R. E. (2016), California tides, sea level, and waves—Winter 2015-16, *Shore Beach*, *84*(2), 25–30.
Flick, R. E., and D. R. Cayan (1984), Extreme sea levels on the coast of California, in *Proceedings of the 19th International Conference on Coastal Engineering*, pp. 886–898, Am. Soc. of Civ. Eng., New York.
Frierson, D. M. W., J. Lu, and G. Chen (2007), Width of the Hadley cell in simple and comprehensive general circulation models, *Geophys. Res. Lett.*, *34*, L18804, doi:10.1029/2007GL031115.
Gemmrich, J., B. Thomas, and R. Bouchard (2011), Observational changes and trends in northeast Pacific wave records, *Geophys. Res. Lett.*, *38*, L22601, doi:10.1029/2011GL049518.
Graham, N. E., and H. F. Diaz (2001), Evidence for intensification of North Pacific winter cyclones since 1948, *Bull. Am. Meteorol. Soc.*, *82*, 1869–1893, doi:10.1175/1520-0477(2001)082 < 1869:EFIONP>2.3.CO;2.
Graham, N. E., D. R. Cayan, P. D. Bromirski, and R. E. Flick (2013), Multi-model projections of 21st century North Pacific winter wave climate under IPCC A2 scenario, *Clim. Dyn.*, *40*, 1335, doi:10.1007/s00382-012-1435-8.
Griggs, G., and K. Brown (1998), Erosion and shoreline damage along the central California coast: A comparison between the 1997-98 and 1982-83 winters, *Shore Beach*, *66*, 18–23.
Hamlington, B. D., S. H. Cheon, P. R. Thompson, M. A. Merrifield, R. S. Nurem, R. R. Luben, and K.-Y. Kim (2016), An ongoing shift in Pacific Ocean sea level, *J. Geophys. Res. Oceans*, *121*, 5084–5097, doi:10.1002/2016JC011815.
Hemer, M. A., Y. Fan, N. Mori, A. Semedo, and X. L. Wang (2013), Projected changes in wave climate from a multi-model ensemble, *Nat. Clim. Change*, *3*, 471–476.
Hines, W. H., and D. C. Montgomery (1980), *Probability and Statistics in Engineering and Management Science*, 634 pp., John Wiley, New York.
Hoskins, B. J., and K. I. Hodges (2002), New perspectives on the Northern Hemisphere winter storm tracks, *J. Atmos. Sci.*, *59*, 1041–1061.
Hu, Y., and Q. Fu (2007), Observed poleward expansion of the Hadley circulation since 1979, *Atmos. Chem. Phys.*, *7*, 5229–5236.
Kalnay, E., et al. (1996), The NCEP/NCAR 40-year reanalysis project, *Bull. Am. Meteorol. Soc.*, *77*, 437–471.
Kumar, A., and M. P. Hoerling (2003), The nature and cause for the delayed atmospheric response to El Niño, *J. Clim.*, *16*, 1391–1403.
Lu, J., G. A. Vecchi, and T. Reichler (2007), Expansion of the Hadley cell under global warming, *Geophys. Res. Lett.*, *34*, L06805, doi:10.1029/2006GL028443.
Mantua, N. J., S. R. Hare, Y. Zhang, J. M. Wallace, and R. C. Francis (1997), A Pacific interdecadal climate oscillation with impact on salmon production, *Bull. Am. Meteorol. Soc.*, *78*, 1069–1079.
Menéndez, M., and P. L. Woodworth (2010), Changes in extreme high water levels based on a quasi-global tide-gauge data set, *J. Geophys. Res.*, *115*, C10011, doi:10.1029/2009JC005997.
Miller, A. J., D. R. Cayan, T. P. Barnett, N. E. Graham, and J. M. Oberhuber (1994), The 1976-77 climate regime shift of the Pacific Ocean, *Oceanography*, *7*, 21–26.
Oort, A. H., and J. J. Yienger (1996), Observed interannual variability in the Hadley circulation and its connection to ENSO, *J. Clim.*, *9*, 2751–2767.
Ralph, F. M., T. Coleman, P. J. Nieman, R. J. Zamora, and M. D. Dettinger (2013), Observed impacts of duration and seasonality of atmospheric-river landfalls on soil moisture and runoff in coastal northern California, *J. Hydrometeorol.*, *14*, 443–459, doi:10.11775/JHM-D-12-076.1.
Schwing, F. B., T. Murphree, and P. M. Green (2002), The Northern Oscillation Index (NOI): A new climate index for the northeast Pacific, *Prog. Oceanogr.*, *53*, 115–139.
Seymour, R. J. (1996), Wave climate variability in southern California, *J. Waterw. Port Coastal Ocean Eng.*, *122*, 182–186.
Sterl, A. (2004), On the (in)homogeneity of reanalysis products, *J. Clim.*, *17*, 3866–3873.
Storlazzi, C. D., and G. B. Griggs (2000), Influence of El Niño-Southern Oscillation (ENSO) events on the evolution of central California's shoreline, *Geol. Soc. Am. Bull.*, *112*(2), 236–249.
Storlazzi, C. D., C. M. Willis, and G. B. Griggs (2000), Comparative impacts of the 1982-83 and 1997-98 El Nino winters on the central California coast, *J. Coast. Res.*, *16*(4), 1022–1036.
Tolman, H. L. (2009), *User Manual and System Documentation of WAVEWATCH III, Version 3.14, Technical Note*, U.S. Dep. of Commer., Camp Springs, Md.
Trenberth, K. E., and J. W. Hurrell (1994), Decadal atmosphere-ocean variations in the Pacific, *Clim. Dyn.*, *9*, 303–319.

Ulbrich, U., G. C. Leckebusch, and J. G. Pinto (2009), Extra-tropical cyclones in the present and future climate: A review, *Theor. Appl. Climatol.*, *96*, 117–131, doi:10.1007/s00704-008-0083-8.

Wahl, T., and D. P. Chambers (2015), Evidence for multidecadal variability in US extreme sea level records, *J. Geophys. Res. Oceans*, *120*, 1527–1544, doi:10.1002/2014JC010443.

Wallace, J. M., and D. S. Gutzler (1981), Teleconnections in the geopotential height field during the Northern Hemisphere winter, *Mon. Weather Rev.*, *109*, 784–812.

Wang, X. L., Y. Feng, G. P. Compo, V. R. Swail, F. W. Zwiers, R. J. Allan, and P. D. Sardeshmukh (2013), Trends and low frequency variability of extra-tropical cyclone activity in the ensemble of twentieth century reanalysis, *Clim. Dyn.*, *40*, 2775, doi:10.1007/s00382-012-1450-9.

Wolter, K., and M. S. Timlin (1998), Measuring the strength of ENSO events—How does 1997/98 rank?, *Weather*, *53*, 315–324.

Zetler, B. D., and R. E. Flick (1985), Predicted extreme high tides for mixed-tide regimes, *J. Phys. Oceanogr.*, *15*(3), 357–359.